Ultra-Wideband Rectenna Using Complementary Resonant Structure for Microwave Power Transmission and Energy Harvesting

Ultra-Wideband Rectenna Using Complementary Resonant Structure for Microwave Power Transmission and Energy Harvesting

Ping Lu, *Member, IEEE*, Chaoyun Song, *Member, IEEE*, and Ka Ma Huang, *Senior Member, IEEE*

***Abstract*— An ultra-wideband (UWB) rectenna (fractional bandwidth > 100%) using a novel wideband complementary matching stub is proposed for microwave power transmission and energy harvesting. A simple resonant structure, i.e., *LC* series–parallel resonant circuit, is embedded to the L-shaped complementary matching stub. Due to the unique frequency response of the *LC* resonant circuit, the proposed matching stub can exhibit "open" and "short" circuits as a function of frequency, thereby acting as a complementary matching circuit covering a relatively wide frequency range. Having utilized the proposed matching stub, the nonlinear input impedance of the rectifier can be tuned to conjugately match the antenna impedance throughout the frequency band of interest. Simulated and measured results show that the proposed rectenna has good matching performance (S_{11} < −10 dB) and high RF-dc conversion efficiency (>50%) over a relatively wide frequency range from 0.9 to 3 GHz (for GSM, Wi-Fi, and WLAN bands). The maximum conversion efficiency of 73.4% is realized at 3-dBm input power. It is evident that the proposed resonant structure-based matching scheme is a promising and effective solution to facilitate the UWB rectenna design with stably high efficiency over a very wide frequency band.**

***Index Terms*— Broadband rectenna, complementary matching stub, microwave power transmission, resonant structure, ultra-wideband (UWB).**

I. Introduction

MODERN wireless communication technologies (4G/5G) will require massive numbers of radio frequency (RF) transmitters to enable wide area and dense coverage of mobile networks, therefore; plenty of mobile base stations have been deployed worldwide in most urban and rural areas. In addition, end-use devices like cellphones will also transmit uplink signals during the communication. As a consequence, diverse RF signals will be widely and densely broadcasted in the ambient environment, and the overall RF power density becomes increasingly large. Ambient wireless signals are typically distributed over a relatively wide spectrum from 800 to 2450 MHz, which roughly covers the frequency bands of GSM900/1800/UTMS/LTE/WLAN. An upsurge of research interest has been devoted to wireless energy harvesting/microwave power transmission (MPT) from ambient mobile signals. With the aid of this emerging energy harvesting/MPT concept, the future generation of maintenance-free and long-term standalone wireless sensors might be achieved, which will enable the reliable operation of passive wireless sensor networks (WSNs) for Internet of Things (IoT) [1]–[4].

Microwave power transmission/wireless energy harvesting is a far-field radiative power transmission (WPT) system that wirelessly transmits power via radio waves. The rectenna, which has been used to receive the radio waves and rectify the RF power to direct current (dc) power, has becoming the most important part of the MPT system. In wireless energy harvesting scenarios, in order to receive RF power from different frequency bands, many broadband and multiband rectennas and rectifiers were proposed [5]–[12]. For example, a coplanar stripline-based broadband rectenna using a broad T-matched dipole and a traditional single-diode rectifier was proposed in [5]. Although the receiving antenna of this example covers a wide frequency band, the rectenna can only achieved high conversion efficiency (>50%) within a very limited frequency range of 1.7–1.8 GHz, which showed that the broadband matching of nonlinear rectifier is very challenging.

Some matching techniques for broadband rectifiers were recently reported; in [6], [7], two inductors are interconnected between the series and shunt diodes of a voltage double rectifier. Using this method, the frequency-dependent capacitance of the rectifying diodes could be largely canceled for realizing wide operational bandwidth. However, the impedance matching between the antenna and rectifying circuit was not fully considered, which will be the wideband matching between two complex impedance values over the frequency range.

Since the complex input impedances of the antenna and rectifier circuit may vary significantly versus frequency, the impedance matching becomes very challenging in broadband rectenna designs [e.g., >30% fractional bandwidth (FBW)]. To achieve good matching performance, some rectennas with multiple and separate matching circuit branches

Manuscript received September 26, 2020; revised December 17, 2020 and February 22, 2021; accepted March 12, 2021. This work was supported in part by the National Natural Science Foundation of China under Grant 51907130 and Grant 61931009; in part by the Sichuan Science and Technology Program under Grant 2020YFH0091; in part by the Chengdu Science and Technology Program under Grant 2020-GH02-00036-HZ; and in part by the Fundamental Research Funds for the Central Universities under Grant 20504153015. *(Corresponding authors: Ping Lu; Chaoyun Song.)*

Ping Lu and Ka Ma Huang are with the School of Electronics and Information Engineering, Sichuan University, Chengdu 610064, China (e-mail: pinglu90@scu.edu.cn; kmhuang@scu.edu.cn).

Chaoyun Song is with the School of Engineering and Physical Sciences, Heriot-Watt University, Edinburgh EH14 4AS, U.K. (e-mail: C.Song@hw.ac.uk).

Color versions of one or more figures in this article are available at https://doi.org/10.1109/TMTT.2021.3067902.

Digital Object Identifier 10.1109/TMTT.2021.3067902

were designed [8]–[10]. Different matching circuit topologies were applied to the circuit branches for covering wider frequency bands, but such a multibranch matching scheme would increase the rectenna size, complexity, and total loss. To miniaturize and simplify the rectenna design, a broadband rectenna with a varactor-based reconfigurable matching stub was proposed [11]. Thanks to the varactor, the matching stub in the rectifier could be reconfigured for realizing good matching between the antenna and rectifying circuit in a wide frequency band. However, an extra biasing network was still required, resulting in difficulties in rectenna integration. Besides, additional loss was introduced by the varactor diode, and the power conversion efficiency was not constantly high in the desired frequency bandwidth. To achieve high conversion efficiency, an off-center-fed (OCFD) asymmetrical dipole with embedded rectifier and a spiral antenna array were proposed for eliminating the matching network to miniaturize the rectenna size further [12], [13]. In [12], the spiral antenna was used as frequency-independent antenna element for a constant source impedance over different frequency bands, while the diode was integrated onto the antenna directly. However, owing to the nonlinearity of the rectifier diode, poor impedance matching between the diode and antenna over a wide frequency band was observed, resulting in low conversion efficiency which varied significantly against frequency. To achieve a stable conversion efficiency over a wide frequency band, the OCFD dipole could provide a constantly high impedance over a wide frequency range, which was helpful to realize a complex conjugate match to the rectifier impedance. But the realized bandwidth of this method was still very limited [13]. Furthermore, both the proposed OCFD dipole and the spiral antenna array were not conventional antennas, leading to the increased complexity of receiving antenna design [12], [13].

Some previous works have shown that by using an *LC* tank, effective conjugate matching to the antenna in the broadband can be achieved to cancel the reactance of the antenna [6], [14]. A parallel or series *LC* tank is implemented for canceling the reactance of the antenna at multiple separate frequency bands, which has a limited capacitive or inductive compensation to the overall broadband antenna system. For a continuously wide operational frequency band, a multistage *LC* circuit might be required, resulting in a complicated broadband matching optimization.

In this article, a novel design method for an ultra-wideband (UWB) high-efficiency rectenna with a resonant structure-based matching stub is proposed. A passive *LC* series–parallel hybrid tank (which is a frequency-dependent impedance transformation circuit) is inserted into the matching stub for simple broadband optimization. The impedance of *LC* tank varies as a function of frequency; therefore, the proposed stub becomes a frequency-dependent matching stub for tuning the rectifier circuit impedance to cancel the inductive and capacitive reactance over a continuously wide frequency band. Particularly, owing to the series and parallel resonant impedance characteristic of the *LC* series–parallel hybrid tank, the stub can be passively connected (short circuit) or disconnected (open circuit) to/from the circuit as a function of frequency for easy tuning

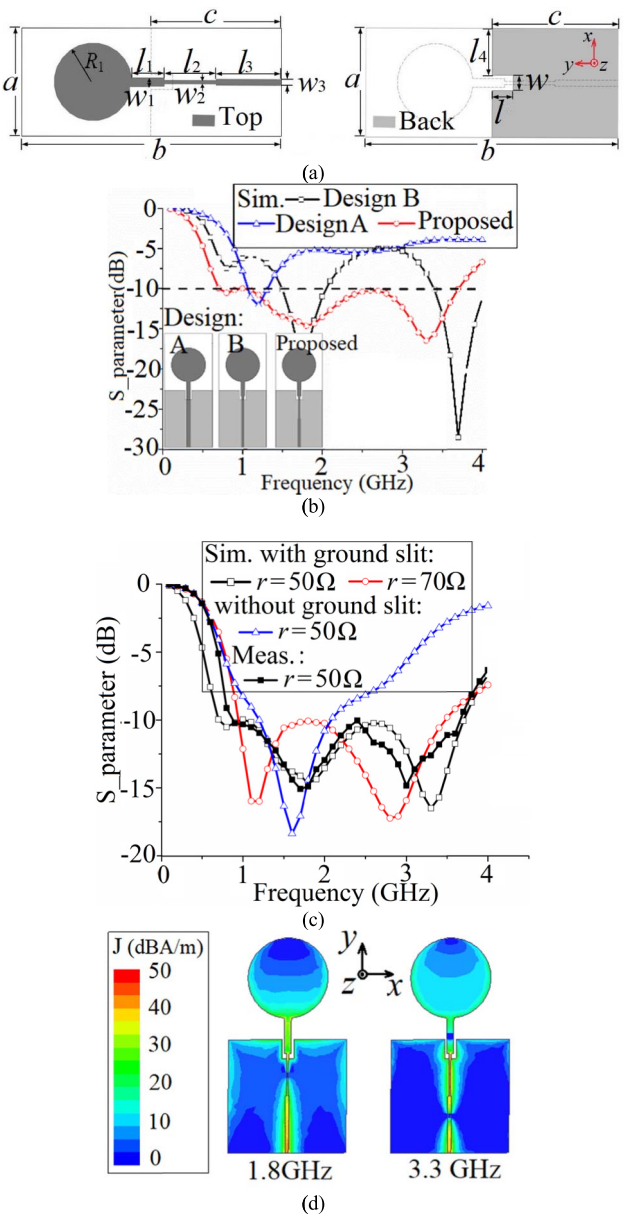

Fig. 1. Proposed receiving antenna. (a) Parameters of receiving antenna: $a = 50$ mm, $b = 100$ mm, $c = 48$ mm, $R_1 = 17$ mm, $w = 5$ mm, $l = 8$ mm, $w_1 = 3$ mm, $l_1 = 15.07$ mm, $w_2 = 0.8$ mm, $l_2 = 18$ mm, $w_3 = 1.5$ mm, $l_3 = 24$ mm, $l_4 = 22.5$ mm. (b) and (c) S-parameter of proposed receiving antenna. (d) Surface current on the receiving antenna.

[15]. Besides, apart from the resonant frequency matching, the rectifier impedance (inductive and capacitive) could be "complementary" to the antenna impedance versus frequency variations. Compared with the broadband rectennas using multiple matching branches [8]–[10], the proposed rectenna has a more compact size. Also, the proposed rectenna can be easily tuned without the need of extra biasing networks [15]. The proposed broadband rectenna with resonator-based complementary matching stub has merits of simplicity, frequency-tuning, and easiness for integration.

II. Broadband Rectenna With Resonator-Based Complementary Matching Stub

The proposed broadband rectenna consists of a circular monopole receiving antenna and a rectifying circuit with

a resonant structure-based matching stub. The antenna and rectifying circuit are integrated on a partially grounded Rogers 5880 substrate ($\varepsilon_r = 2.2$, $\tan\delta = 0.0009$).

A. Broadband Receiving Antenna Structure

To achieve wideband operation, the receiving antenna is designed based on a planar monopole. The receiving antenna contains a circular patch with a radius of R_1 and a feeding line with three matching sections, as displayed in Fig. 1(a), where the antenna is printed on the top side of the Rogers 5880 substrate with a thickness of $h = 0.787$ mm. On the top side of the substrate, the radius of the circular patch can be found for the center frequency [16]. For numerous broadband impedance matching techniques, existing methods including feedgap optimization between the ground and circular patch, the ground slits, and the microstrip feedline transitions are used [17]–[20]. In this design, the three-section microwave transitions are used to match the circular patch to the feedline, and a quadrate slit with a size of $l \times w$ is etched at the partial metallic ground ($a \times c$) on the back side of the substrate. By implementing multisection transitions with different sizes, the operating bandwidth can be extended [19]. After investigation, two structures were simulated by using a single (Design A) and a dual microstrip line transitions (Design B), as displayed in Fig. 1(b). It can be seen that without using the microstrip line transitions (Design A), the simulated bandwidth ($|S_{11}| < -10$ dB) of 1.1–1.3 GHz [FBW is 16.6%] is obtained, which is very narrow. For a dual-section transition, the simulated bandwidths ($|S_{11}| < -10$ dB) of 1.6–2 GHz (FBW = 22.2%) and 3.4–4 GHz (FBW = 16.2%) are obtained, and the bandwidth is extended. For a three-section transition (the proposed antenna), the simulated bandwidth becomes 0.8–3.7 GHz (FBW = 128.8%) which is extremely wide. Also, the ground quadrate slit is adopted to reduce the lower edge resonant frequency and widen the higher edge frequency for enhancing the broadband impedance matching further [see in Fig. 1(b)] [18].

The current distributions at two major resonances (the minimums in $|S_{11}|$) of 1.8 GHz (low-frequency band) and 3.3 GHz (high-frequency band) are also given in Fig. 1(b). It can be observed that the currents on the back side ground plane are mainly concentrated near the edge of the ground plane (closest to the circular disk), while on the top side of the antenna structure, the currents are primarily distributed along the periphery of the circular disk edge and feedline [16], [20], [21]. Radiating slots can be thought to form between the lower edge of the circular disk and ground plane with the slit [22]. For instance, at 1.8 GHz, the distinct maxima of the current can be observed at the junction of the feedline and the circular disk and the edge of the ground plane (closest to the circular disk), while at 3.3 GHz, one distinct maxima is distributed on the circular disk and the feedline. These different current distributions can also signify particular modes of antenna operation: at lower frequencies (1.8 GHz), monopole antennas can be thought to function in an oscillating or standing wave mode, and with an increase in frequency, operation develops into a hybrid of both standing and traveling wave (at 3.3 GHz) [16].

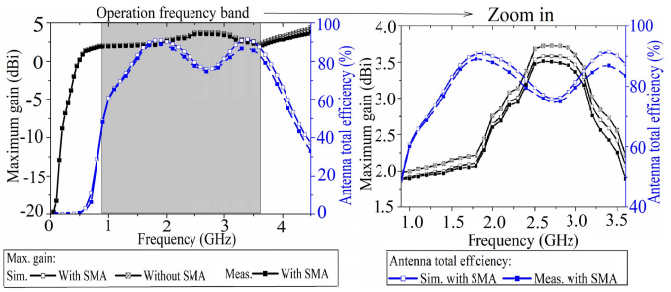

Fig. 2. Maximum gain and antenna efficiency of the proposed receiving antenna. Figure on the right: maximum gain and antenna efficiency within the operation frequency band are zoomed in.

The measured reflection coefficient $|S_{11}|$ is also depicted in Fig. 1(b). It can be clearly seen that the measured impedance bandwidth (for $|S_{11}| < -10$ dB) becomes a bit narrower, which is from 0.9 to 3.6 GHz. It covers the GSM 900/1800, UMTS2100, and 2450-MHz WLAN bands. The frequency offset may be attributed to the deviation of the dimensional error and the substrate permittivity. Also, it is found that the substrate permittivity with a 2% drop is slightly lower than that used in the simulation, resulting in the higher frequency than expectation. Considering that a standard 50-Ω female SMA connecter was used in the measurement, the reference impedance of the antenna port was set to be 50 Ω in the simulation, of which the impedance is different from the characteristic impedance bandwidth of the microstrip feedline (about 70 Ω). By simulation, the port impedance r varying from 50 to 70 Ω against different frequencies is displayed in Fig. 1(b), where the frequency bandwidth becomes narrow at $r = 70$ Ω. However, this problem will not affect the rectenna design as the rectifier and antenna will be co-designed using the microwave feedline and matching stub in the later stage, rather than the SMA connecter. Although the discrepancy of S-parameter between the simulation and measurement exists, especially the shift in the resonant frequency at high frequency, the desired band for wireless communications is fully covered and the measurement agrees reasonably well with the simulated one.

In this design, the tradeoff between high gain and compact size is considered. For more received power, the proposed circular monopole UWB antenna using typical shape would outperform other modified slot antennas and coplanar waveguide (CPW) antennas, as the gain of those antennas could be lower [23]. The simulated (measured) maximum gain G_r of the proposed antenna in the operating bandwidth of 0.9–3.6 GHz is from about 1.98 dBi (1.88 dBi) at 0.9 GHz to 3.73 dBi (3.51 dBi) at 2.7 GHz (2.6 GHz), as displayed in Fig. 2, where the maximum gain can be observed at 2.7 GHz (2.6 GHz), and then decreases as a function of frequency. The measured gain is slightly lower than the simulated one, which might be due to the absence of SMA connector in our simulation. After further investigation, we found that the SMA indeed has some impacts on the antenna gain, as shown in the simulated gain with and without using the SMA connector (see Fig. 2). In addition, it should be noted

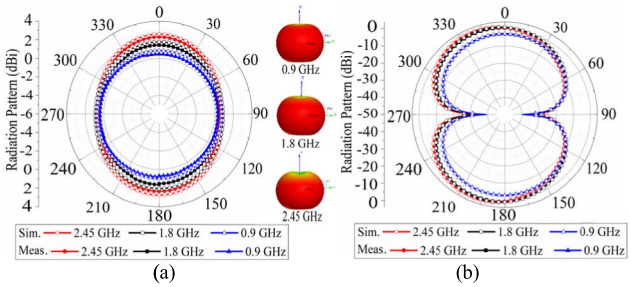

Fig. 3. Radiation Patterns of the proposed receiving antenna at 0.9, 1.8, and 2.45 GHz. The 3-D radiation patterns are illustrated. (a) *XOZ* plane. (b) *XOY* plane.

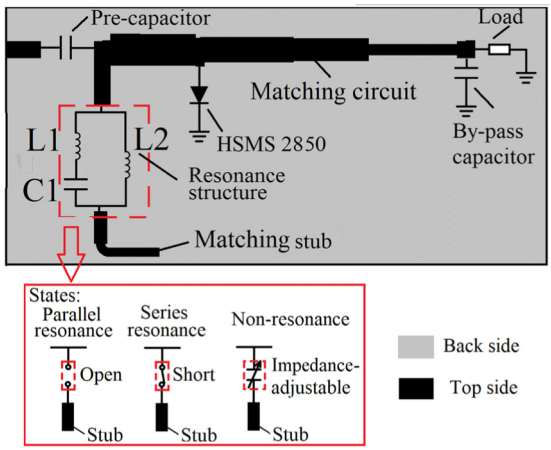

Fig. 4. Proposed rectifying circuit structure with equivalent circuit of *LC* tank in different states.

that it will be difficult to measure the efficiency of UWB antennas accurately. Therefore, our antenna efficiency was measured in a reverberation chamber (RC) using three-antenna methods rather than two-antenna methods in the anechoic chamber [24]. The RC will evaluate the antenna efficiency without considering the antenna orientation and misalignment, therefore, giving more precise efficiency results, especially for UWB antenna tests. From Fig. 2, it can also be seen that the simulated (measured) antenna total efficiency η_a reaches up to 48.89% (48.12%)–90.88% (89.15%), as displayed in Fig. 2, where the antenna total efficiency increases as a function of frequency, and then decreases as frequency beyond 3.5 GHz. The reduction in the measured gain (antenna efficiency) might be caused by the actual loss of the SMA connector, about 0.08–0.29 dB at the operation frequency band of 0.9–3.6 GHz in the measurement, which is larger than the simulated loss (0.06–0.11dB). Besides, the radiation patterns at the frequency of 0.9, 1.8, and 2.45 GHz are shown in Fig. 3. Despite the slight deviation between the simulation and measurement, the two results are in good agreement.

B. Rectifying Circuit With Resonator-Based Matching Stub Structure

A rectifying circuit with a resonant structure-based matching stub is proposed for a wide frequency band, as shown in Fig. 4. The proposed rectifying circuit, composed of a precapacitor, a shunt rectifier diode, a bypass capacitor, a frequency-adjustable microstrip stub with an *LC* tank, a matching circuit, and a load, is printed on the same PCB substrate of the antenna. The precapacitor of 330 pF protects the receiving antenna from the reverse rectified dc current. A Schottky diode HSMS 2850 with a breakdown voltage V_{br} of 3.8 V, a built-in voltage V_{bi} of 0.35 V, a series resistance R_s of 25 Ω, and a junction capacitance C_{j0} of 0.18 pF is used as a rectifier diode to insert into the rectifying circuit using a shunt connection for low/medium power [2], [25]. A bypass capacitor of 100 pF is used as an output filter, not only to smooth the voltage waveforms, but also to suppress the high-order harmonics in cooperation with the precapacitor. The matching circuit has several stepped-impedance matching microstrip lines. A microstrip stub with a resonant structure is located between the antenna and the rectifier to achieve broadband impedance matching.

C. LC Tank Resonant Structure Design

It is well known that the input impedance of nonlinear circuits varies significantly with the operation frequency. To achieve high conversion efficiency, the value of the antenna impedance $(R - jX)$ Ω should conjugately match with the input impedance of a specific rectifier $(R + jX)$ Ω within a desired frequency range [13]. For a wideband rectenna, it is difficult for a conventional rectifying circuit to achieve good conjugate match in the broadband, resulting in the low and unstable conversion efficiency over a wide frequency range. In the proposed rectifying circuit, an *LC* tank resonant structure is implemented in series to an L-shaped stub, which is inserted between the precapacitor and rectifier to construct a frequency-dependent matching stub for achieving impedance complementary over a wide frequency range. Due to the intrinsic characteristic of the *LC* resonator, the impedance of a series or shunt *LC* tank varies with different frequencies; hence, the *LC* tank can be modeled as a frequency-dependent impedance transformation circuit. Specifically, when a capacitor is in series (parallel) connection with an inductor, the *LC* tank could become a short (open) circuit at a certain series (parallel) resonance frequency of $f_0 = 1/2\pi\sqrt{LC}$. In resonance states, the L-shaped stub can be electrically connected to (disconnected from) the rectifying circuit, and it can be equivalently modeled as the ON-state (OFF-state) switch-based reconfigurable stub [15]. Accordingly, as the frequency changes, the *LC* tank can mimic an open circuit (at parallel resonance), a short circuit (at series resonance), and an impedance-variation circuit (nonresonance), and the L-shaped stub becomes a frequency-dependent matching stub, as displayed in Fig. 4.

The output impedance of the proposed antenna $(Z = R + jX)$ Ω is displayed in Fig. 5(a), where the real part $(Z = R)$ of the impedance ranges from 4.3 to 92.5 Ω in the frequency range of interest. The imaginary part of the antenna impedance,first changes from inductive $(Z = jX,\ X > 0)$ to capacitive $(Z = jX,\ X < 0)$ and goes back to inductive in the frequency band of 0.9–2.7 GHz, and then slopes downward to the capacitive impedance at 2.8–3.4 GHz, and eventually

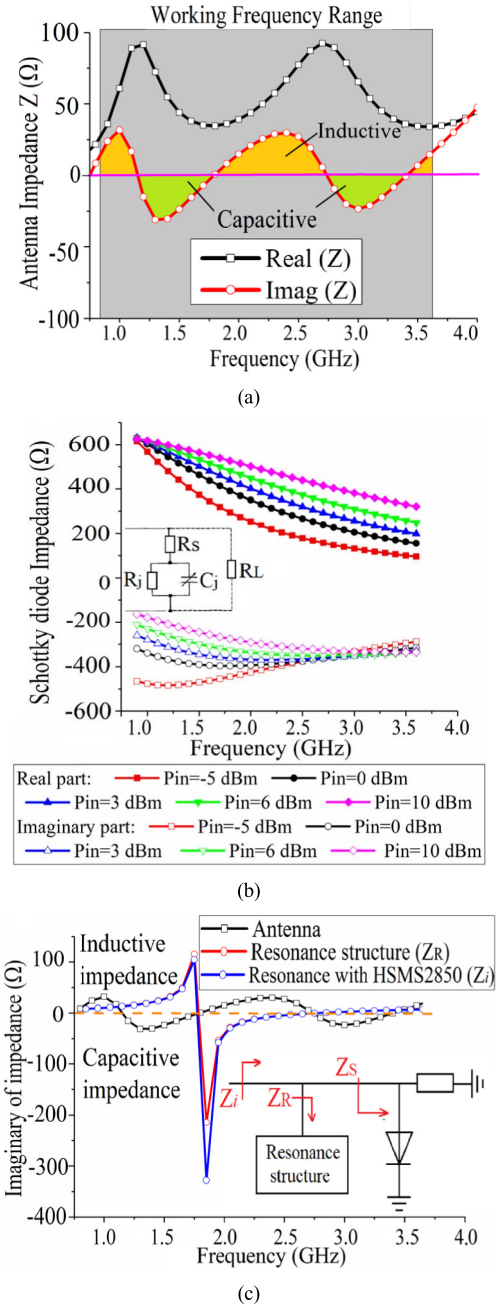

Fig. 5. Impedance with different frequencies. (a) Antenna impedance. (b) HSMS2850 diode impedance Z_s with 1-kΩ load at different input powers of −5, 0, 3, 6, and 10 dBm. The equivalent circuit of Schottky diode with a load is illustrated [29]. (c) Imaginary part of the antenna, resonance structure, and resonance with HSMS 2850 (at input power of 3 dBm). The equivalent circuit of the rectifying circuit topology with resonance structure is illustrated.

turns back to inductive behavior as the frequency increases further. Within the desired working frequency range of 0.9–3.6 GHz, the imaginary part of the antenna impedance crosses through zero at the frequency of 1.8, 2.75, and 3.45 GHz [see Fig. 5 (a)]. For high conversion efficiency, the impedance of the rectifying circuit should conjugately match to antenna impedance.

Due to the nonlinearity, the impedance of HSMS 2850 using load $R_L = 1$ kΩ varies with different frequencies of 0.8–4 GHz at different input powers of −5, 0, 3, 6, and 10 dBm, as displayed in Fig. 5(b). It can be found that both real and imaginary parts of the diode impedance are a nonlinear function of frequency. The real part of the impedance decreases from 600 Ω as the frequency increases, while the imaginary part of the impedance of the HSMS 2850 diode is always kept capacitive (<0 Ω). And it is obvious that the antenna impedance changes between the capacitive and inductive; thus, it is difficult to use a single matching stub to achieve the conjugate matching between the antenna and the rectifier over wide frequency bands, and several matching stubs are required for multiband conjugate matching.

In this design, the *LC* series–parallel hybrid tank is used to avoid several matching stubs. A single inductor (L_1) and a single capacitor (C_1) are serially connected with an alternative inductor (L_2) connected in parallel to the series *LC*. The input impedance of the proposed *LC* tank can be expressed by

$$Z = \frac{j\omega L_2(1-\omega^2 L_1 C_1)}{1-\omega^2 C_1(L_1+L_2)}. \tag{1}$$

It can be seen that when the capacitance and inductance are constant, the impedance of the *LC* tank varies with the frequency. When the *LC* hybrid tank works in resonant mode, the series (parallel) resonance frequency of f_{01} (f_{02}) can be derived by

$$\begin{cases} f_{01} = 1/2\pi\sqrt{L_1 C_1}, & \text{Series Resonance} \\ f_{02} = 1/2\pi\sqrt{C_1(L_1+L_2)}, & \text{Parallel Resonance.} \end{cases} \tag{2}$$

For the RLC circuits, the limits of broadband bandwidth can be found [26]–[28]

$$\frac{\Delta\omega}{\omega_c}\ln\frac{1}{r_{\max}} < k\frac{\pi}{Q} \tag{3}$$

where

$$k = \begin{cases} \omega_c/\omega_0 & \text{for } \omega_c < \omega_0 \\ 1 & \text{for } \omega_c = \omega_0 \\ \omega_0/\omega_c & \text{for } \omega_c > \omega_0. \end{cases} \tag{4}$$

The resonant frequency of the circuit is ω_0, and Q is the figure of merit, which can be expressed by $Q = R\omega_0 C = R/\omega_0 L$. r is the scattering matrix, i.e., $|S_{11}(j\omega)| = |S_{22}(j\omega)| = r$. ω_c is the center frequency of the desired matching interval, i.e., $\omega_c = (\omega_1\omega_2)^{1/2}$, where ω_1 is the lower cutoff frequency and ω_2 is the upper cutoff frequency. It is noted that the center frequency ω_c is not necessarily equal to the resonant frequency ω_0. $\Delta\omega = \omega_2 - \omega_1$. For the proposed *LC* series–parallel hybrid tank, which is represented by RLC series circuit with the addition of RLC parallel circuit, the maximum FBW can be obtained

$$\begin{cases} 2.7R\sqrt{C_1/L_1}, & \text{RLC series circuit} \\ 2.7/R\sqrt{(L_1+L_2)/C_1}, & \text{RLC parallel circuit.} \end{cases} \tag{5}$$

It is worth noting that R is the equivalent resistance value of the rectifying circuit part behind the *LC* tank stub (including main multisection matching network and HSMS 2850 with bypass capacitor and the load). However, the impedance of the rectifying circuit part behind the *LC* tank stub is generally

a complex number, and its imaginary part can be equivalent to an additional shunt elements L' or C'. In this case, the maximum FBW for the RLC parallel circuit becomes $2.7/R((L_1+L_2')/C_1)^{1/2}$, where $L_2' = L_2//L' = L_2L'/(L_2+L')$ for the shunt element L' or $L_2' = L_2//C'$ for the shunt element C'. Hence, the proposed LC series–parallel hybrid tank is the union of the maximum FBW for the series circuit and that of the parallel circuit.

According to the antenna impedance curve [see Fig. 5(a)], the series resonance frequency f_{01} of 2.75 GHz and the parallel resonance frequency f_{02} of 1.8 GHz can be chosen for good matching. To realize the two resonance frequencies, many values of inductance and capacitance can be selected from the surface-mounted device (SMD) components. Considering the off-the-shelf parts from the supplier, the LC series–parallel hybrid tank can be build using i.e., $C_1 = 3.3$ pF (Model: GCM1885C1H3R3CZ13), $L_1 = 1$ nH (Model: LQG15HN1N0S02), and $L_2 = 1.3$ nH (Model: LQG15HN1N3S02), according to the calculation given in (2). The frequency dependence of reactance (imaginary part) of the proposed LC tank is displayed in Fig. 5(c), where the rectifying circuit topology with resonance structure is displayed. The input impedance Z_i of the rectifying circuit topology without any microwave strip matching network can be expressed by

$$Z_i = Z_R//Z_s = Z_R Z_s/(Z_R + Z_s) \tag{6}$$

where Z_S is the impedance of the HSMS 2850 with the load, which is 1 kΩ in the design and Z_R is the impedance of the resonance structure. The imaginary part of input impedance (Z_i) with different frequencies is also shown in Fig. 5(c). It can be seen that the impedance of the LC tank/rectifying circuit topology is inductive within the frequency band of 0.9–1.8 GHz, and then it mutates to become capacitive after the parallel resonant frequency of 1.8 GHz. As the frequency increases further, the impedance gradually changes to the inductive values, where the imaginary part of the impedance crosses the zero at the series resonant frequency of 2.75 GHz. It can be observed that the trend of the impedance variation with LC tank/rectifying circuit topology is complementary to that of the imaginary part of antenna impedance. Besides, with the LC tank resonance-based stub, the real part of the rectifying circuit topology Z_i (0–68.8 Ω) is much lower than that of HSMS 2850 Z_S (95–630 Ω), and it is closer to the real part of antenna (4.3–92.5 Ω). Hence, it is helpful to get the impedance of antenna conjugate matched to that of the rectifying circuit in a wide frequency range with low insertion loss by using a simple matching circuit, i.e., the matching microstrip stub in the complementary stub and multisection matching network in the proposed design.

D. Conversion Efficiency

The conversion efficiency η_c of the rectifying circuit can be written by

$$\eta_c = \frac{V_{\rm dc}^2}{P_{\rm in} R_L} = \frac{V_{\rm dc}^2}{R_L} \cdot \frac{(4\pi L)^2}{G_t G_r P_t \lambda^2 \eta_a} \tag{7}$$

where $V_{\rm dc}$ is the output dc voltage across the load R_L, and $P_{\rm in}$ is the input power of the rectifying circuit. The second equation on the right-hand side is calculated using the Friis transmission equation, where G_t and G_r are the gains of the transmitting antenna and the receiving antenna, respectively, P_t is the transmitted power of the transmitting antenna, L is the distance between the transmitting antenna and the rectenna, and η_a is the antenna efficiency.

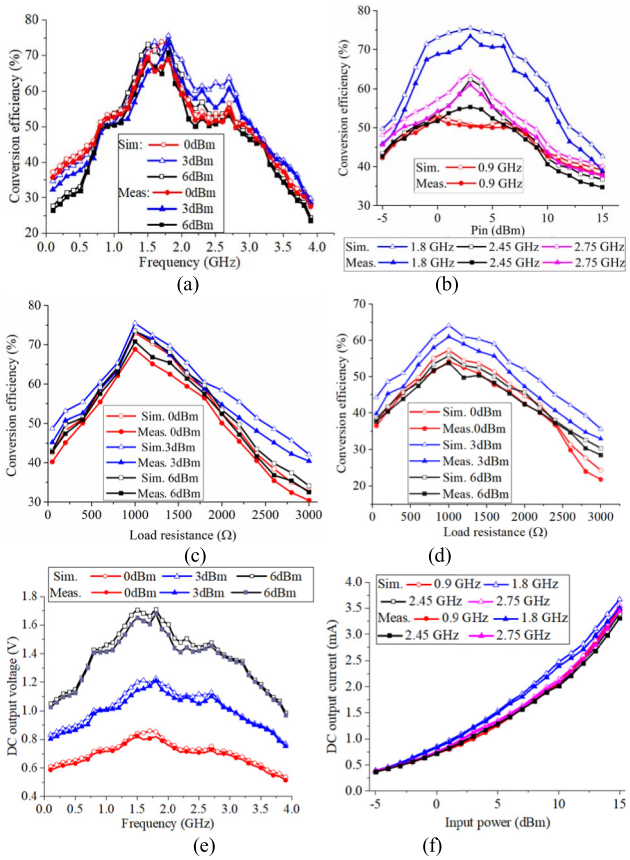

Fig. 6. Simulated and measured conversion efficiency of the rectifying circuit with different input powers at different frequencies. (a) Conversion efficiency versus frequency at three input powers over the load resistance of 1 kΩ. (b) Conversion efficiency versus input power level at three frequencies over the load resistance of 1 kΩ. (c) Conversion efficiency versus load resistances at three input powers at 1.8 GHz. (d) Conversion efficiency versus load resistances at three input powers at 2.75 GHz. (e) DC output voltage with different frequencies. (f) DC output current with different input powers.

To take the matching between the antenna and rectifying circuit into full consideration, the rectenna was co-simulated using HFSS and ADS software. A power source is used to replace the antenna port in the rectifier simulation. The internal impedance of the single tone power source was written in SIP file, which is the Z-parameter of the antenna exported from HFSS, where the port is not renormalized.

The simulated conversion efficiency at different frequencies with different input powers and load resistances can be displayed in Fig. 6. It can be seen that, due to the nonlinearity of HSMS 2850, maximum conversion efficiency of 75.5% can be achieved at the frequency of 1.8 GHz with an appropriate load resistance R_L of 1 kΩ and an optimum input power of 3 dBm. The detailed data of the conversion efficiency can be found in Section III.

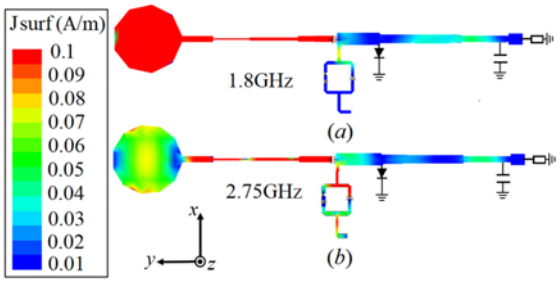

Fig. 7. Surface current distributions (magnitude) on the rectenna structure. (a) At the parallel resonance frequency of 1.8 GHz. (b) At the series resonance frequency of 2.75 GHz.

E. Design Guideline of Matching Circuit

Through the above analysis, the details of the *LC* resonant tank can be determined by the imaginary part of antenna impedance, and it is helpful for the rectifying circuit to cancel out the capacitive or inductive reactance of the antenna for impedance complementing. Then, by tuning the matching circuit of the rectifying circuit, good matching can be achieved between the receiving antenna and the rectifying circuit.

To help engineers understand the design process of the proposed matching circuit, the design guidelines are given as follows.

Step 1: Main matching circuit of the rectifying circuit design. At the parallel resonant frequency of 1.8 GHz, the proposed *LC* tank is equivalent to an open circuit, and accordingly the L-shaped stub is disconnected from the rectifying circuit. The surface current (magnitude) distributions at 1.8 GHz is displayed in Fig. 7(a), where the latest electromagnetic (EM) simulators in ADS (version 2020) were used for simulating the current distributions on the rectenna with SMDs i.e., inductor and capacitor. It can be seen that the dominant current at 1.8 GHz is mainly distributed over the circular patch, feedline and main circuit branch of the rectifying circuit, and fewer current flows through the shunted stub. By adjusting the size of the stub, we found that the rectenna performance is barely changed, but the proposed *LC* tank exhibits capacitive characteristics to cancel the inductive reactance of the antenna at 1.8 GHz. Subsequently, the main matching circuit (on the horizontal branch) plays a leading role in the conjugate match. A two-section microstrip line is used. One section of the microstrip line is used to cancel the redundant capacitance characteristics of the imaginary part, and the other section is used to achieve good matching to the real part of the antenna impedance. Thus, the two-section microstrip line is tuned, and the input impedance of the rectifying circuit reaches $(36.54 - j0.21)\ \Omega$ at 1.8 GHz, which is complementary to the impedance of antenna $(34.7 + j0.79)\ \Omega$, as listed in Table I, where the optimum input power of 3 dBm for the rectifying circuit is chosen.

Step 2: L-shaped stub design. At the series resonance frequency of 2.75 GHz, the proposed *LC* tank is equivalent to a short circuit, and then L-shaped stub is connected to the rectifying circuit. Also, the surface current (magnitude) distribution at 2.75 GHz is extracted, as shown in Fig. 7(b).

TABLE I

SIMULATED IMPEDANCE OF THE PROPOSED RECTENNA AT DIFFERENT FREQUENCIES AT INPUT POWER OF 3 dBm

Freq. (GHz)	Input impedance of antenna (Ω)	Input impedance of rectifying circuit (Ω)	Conversion efficiency (%)
0.9	21.72+*j*8.45	37.45-*j*15.4	50.8
1.2	91.54-*j*15.09	76.87+*j*12.14	57.1
1.5	43.9-*j*23.65	38.1+*j*20.53	72.1
1.8	34.7+*j*0.79	36.54-*j*0.21	75.5
2.1	43.67+*j*20.90	52.9-*j*17.2	63.8
2.4	66.88+*j*29.88	77.8-*j*26.3	60.4
2.7	92.5+*j*5.71	84.4-*j*4.57	63.7
2.75	90.5+*j*4.71	89.4-*j*4.27	64.1
3	65.4-*j*23.43	78.54+*j*29.54	51.4
3.3	39.62-*j*8.11	59.48+*j*12.65	43.1

The complementary stub has sensible impact on the rectenna performance at 2.75 GHz, from which we can observe that significant current is distributed at the antenna circular patch, feedline, main circuit branch of the rectifying circuit, and the shunted complementary stub. Hence, good matching can be achieved with the aid of the complementary stub and the main matching circuit of the rectenna (multisection matching circuit of the antenna and rectifying circuit). To ensure good performance at 1.8 GHz, the main matching circuit almost keeps unchanged, and the complementary stub dominates the matching at 2.75 GHz. At this frequency, the imaginary part of the antenna is close to 0 Ω, and the complementary stub size is largely used for the rectifying circuit to match to the real part of the antenna, cooperated with the main matching circuit network. By controlling the size of the L-shaped stub, the impedance of the rectifying circuit is adjusted to $(89.4 - j4.27)\ \Omega$, and it can match well with the antenna impedance of $(90.5 + j4.71)\ \Omega$, as displayed in Table I.

Step 3: Fine-tune the entire rectifying circuit. As displayed in Fig. 8(a), two-section microstrip line is still used for multiple separate frequency bands. Hence, the multisection microstrip line is used for broadband operation. Having conducted the fine-tuning of the *LC* tank stub and multisection matching network, the impedance of the rectifying circuit is conjugated to the antenna impedance for high conversion efficiency within the operational wide frequency range [30].

Due to the frequency dependence of the proposed *LC* resonant tank [see Fig. 5(c)], the L-shaped stub becomes a frequency-tuning matching stub. From Fig. 7, the current distributions at different frequencies validate that the added *LC* tank-based stub has frequency-dependent complementary function to compensate the overall impedance matching of the rectenna within the frequency band of interest. The conjugate match can be effectively achieved in the proposed rectenna, and the detail impedances of the rectenna at different frequencies are listed in Table I, where the input impedance of antenna and rectifier can be extracted using the HFSS and ADS, respectively.

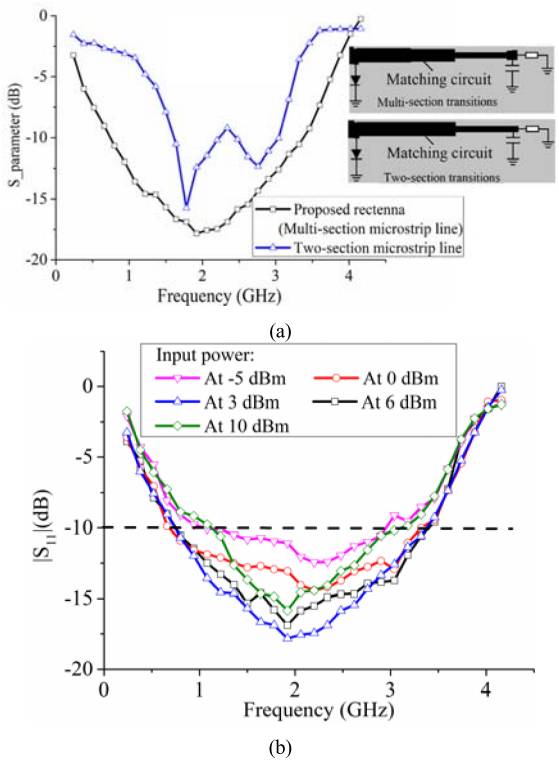

Fig. 8. Simulated $|S_{11}|$ of the proposed rectifying circuit with different frequencies over the load resistance of 1 kΩ. (a) With multisection and two-section microwave lines at the input power of 3 dBm. (b) At the input power of −5–10 dBm.

The S-parameters of the rectifying circuit versus the operation frequency at different input powers are simulated, as displayed in Fig. 8(b), where the proposed rectifying circuit can provide good input return loss ($|S_{11}| < -10$ dB) over the frequency band of 0.8–3.3 GHz and the input power range from 0 to 6 dBm, indicating that the proposed rectenna can achieve good impedance matching performance in these frequencies and at input power ranges. When the input power increases or decreases further, since the impedance matching deteriorates, the operation frequency band of rectifying circuit becomes narrow, which is 1.1–2.9 GHz at −5 dBm and 1.2–3 GHz at 10 dBm, respectively. It is worth noting that the reflection coefficient is lowest in the frequency range of interest at the input power of 3 dBm; hence, 3 dBm is verified to be the optimal input power of the proposed rectifying circuit, as displayed in Fig. 6(b).

III. Performance of Resonance-Based Rectenna

The fabricated prototype rectenna is shown in Fig. 9, where the receiving antenna and the rectifying circuit are electrically connected using the microstrip line and printed on a partially grounded Rogers 5880 substrate. As displayed in Fig. 9, a truncated area is formed, since the antenna size (length × width) differs from the rectifying circuit size. However, the rectifier size can be increased to fill the absent area without changing the performance significantly, since the rectifier is nonradiating element [31]. We used identical sizes to the simulated models for the antenna and rectifier, therefore, getting a good result

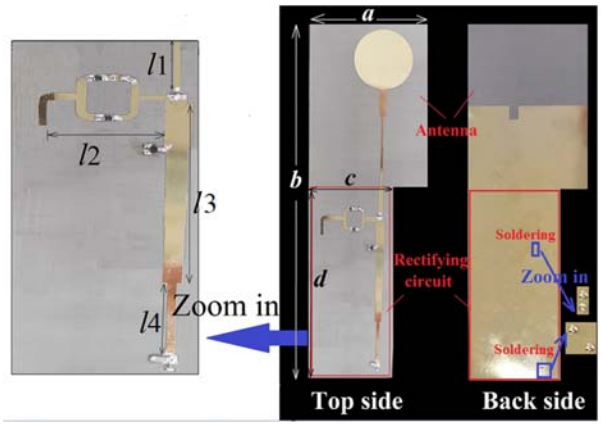

Fig. 9. Fabricated rectenna (a = 60 mm; b = 200 mm, c = 38 mm, d = 100 mm; l_1 = 16.1 mm; l_2 = 29.8 mm; l_3 = 59.6 mm; l_4 = 22.9 mm).

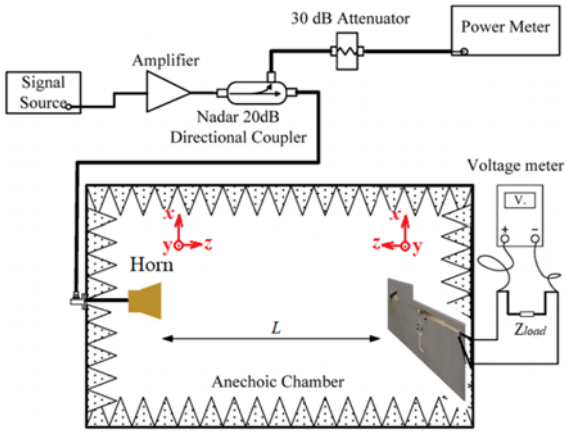

Fig. 10. Measurement setup in the anechoic chamber. The signal source (modeled Agilent 83623L) was used to generate RF power, and the RF power was magnified by an amplifier. Then, the amplified RF power was shunted by a Nadar 20-dB directional coupler. One way feeds the transmitting horn, while another way feeds the power meter of Agilent E4416A to test the transmitting power. The rectenna is placed at the distance of L from the transmitting horn. A multi-meter measures the output voltage across the load of the rectenna.

alignment. The overall performance of the rectenna would typically not be affected by the truncated area.

The measurement setup of the proposed rectenna is displayed in Fig. 10. In the measurement, the load was chosen as 1 kΩ, and L was 2.5 m. Three standard gain horn antennas (model: QSH5#10 for 0.9–1.5 GHz with G_t of 10 dBi, QSH7#10 for 1.4–2.2 GHz with G_t of 10 dBi, and QSH9A#15 for 2.2–3.3 GHz with G_t of 15 dBi) were used for P_t of 0.72–7.46 W covering the frequency band of 0.9–3.3 GHz, as P_{in} was configured at 0–6 dBm (0.01–0.3 mW/cm^2), which was much smaller than the safety standard of 1 mW/cm^2. The proposed power level of 0–6 dBm can be satisfied when the device location is close to multiple RF power sources (e.g., base station, signal tower), and the captured energy can be used to power remote devices in WSN, RF Identification (RFID), and environmental sensing for low continuous power supplies.

The simulated and measured conversion efficiency versus different frequencies at 0–6-dBm power is displayed in

Fig. 6(a), where the measured results agree well with the simulated ones. The simulated/measured conversion efficiency of $\eta_c > 50\%$, (up to 75.5%/73.4% at 1.8 GHz) can be achieved over the desired broad frequency from 0.8 to3 GHz/0.9 to 3GHz for the optimum input power level of 3 dBm. When the input power is doubled (6 dBm) or halved (0 dBm), simulated/measured high efficiency ($\eta_c > 50\%$, up to 73.5%/70.8% at 6 dBm or 73%/68.8% at 0 dBm at 1.8 GHz) is still realized over the band of 0.9–2.8 GHz. Since the matching network is optimized at 1.8 GHz (low-frequency band) and 2.75 GHz (high-frequency band), highest conversion efficiency was achieved at these two (i.e., low and high) frequency bands. Due to the frequency-dependent loss of the components (i.e., SMD components and rectifier diode) in the rectenna, the conversion efficiency at low frequency of 1.8 GHz is higher than that at high frequency of 2.75 GHz. Also, the simulated and measured conversion efficiency of the rectenna versus input power level is shown in Fig. 6(b) at the four frequencies of 0.9, 1.8, 2.45, and 2.75 GHz. It can be seen that the conversion efficiency varies with different input powers and frequency bands, and the proposed rectenna has high conversion efficiency ($\eta_c > 50\%$) under the input power of around 0–6 dBm at the four frequencies, where good impedance matching can be achieved. In practice, the dc load variation may exist over a large range in different scenarios; thus, it is necessary to reduce the sensitivity of efficiency versus load resistances. The simulated and measured conversion efficiency with different load resistances at the parallel/series resonance frequency of 1.8/2.75 GHz can be displayed in Fig. 6(c) and (d), where the three input power levels of 0, 3, and 6 dBm are chosen. It can be seen that the conversion efficiency keeps constantly high (above 50%) at 1.8/2.75 GHz for the load resistance between 400 Ω/800 Ω and 2000 Ω/1500 Ω, especially for the load values of 200–2200 Ω/600–1800 Ω at the optimum input power of 3 dBm, demonstrating that the nonlinear effect is reduced over the load range from 400 to 2000 Ω/800 to 1500 Ω. While the load resistance increases further, the conversion efficiency starts to decrease, due to the impedance mismatch between the antenna and the rectifying circuit. Furthermore, dc output voltage with different frequencies and dc current with input power are displayed in Fig. 6(e) and (f), respectively. Since the dc output current can be found by $I_{\text{out}} = V_{\text{out}}/R_L$, the variation tendency of the dc output voltage is identical to that of dc current. As displayed in Fig. 6(e), it can be found that, at the input power levels of 0, 3, and 6 dBm, the simulated/measured output voltage increases with frequency, and it reaches a maximum of 0.85/0.82, 1.23/1.21, and 1.71/1.68 V at the operation frequency of 1.8 GHz, and then decreases with frequency increasing further. At the high-frequency band of 2.3–4 GHz, another maximum voltage can be achieved at 2.75 GHz. As displayed in Fig. 6(f), at different frequency, dc output current increases with different input powers. Besides, dc output current at 1.8 GHz is highest among those at other frequencies. In the practical system, the voltage can be further regulated using dc–dc converter, which can be used to match the rectenna to its optimal load condition and maintain high conversion efficiency against dynamic operating conditions [32]. According to the results in Fig. 6, the proposed rectenna can work well ($\eta_c > 50\%$) under the input power of 0–6 dBm at the broadband of 0.9–2.8 GHz over the load resistance of 800–1500 Ω. Under these conditions, the nonlinear effect decreases and good impedance matching between the antenna and rectifying circuit can still be achieved. The measured results are lower than the simulated ones. The discrepancy is due to the actual parasitic elements of the SMD components (i.e., capacitors and inductors) and rectifier diode, which is different from the SPICE mode in the ADS simulation, resulting in slightly worse impedance matching.

TABLE II
COMPARISON OF BROADBAND RECTENNAS AND RECTIFIERS

Ref.	Freq. band for η_c >50% (GHz)	Size of rectenna (cm^2)	Max. Eff. (%) @ P_{in} (dBm)	P_{in}(dBm) /R_L (Ω) range for η_c >50%
[5]	1.7~2.4	9×4.7 (0.51λ×0.27λ@ 1.7 GHz)	62.4@-2.5	-2.5/857
[6]	0.54~1.3	6.69×1 (rectifier) (0.12λ×0.02λ@ 0.54 GHz)	80@10	-5~10 /14000
[7]	0.1~2.5 (>45%)	2.25×3.1(rectifier) (0.0075λ×0.01λ @0.1 GHz)	74.8@10	-15~20 /1000
[8]	1.8~2.5	7×7 (0.42λ×0.42λ@ 1.8 GHz)	55@-10	-10~0 /14700
[9]	1.8~2.2	38×24.7 (2.28λ×1.4λ@1.8 GHz)	50@-10	-10~-5 /5000
[10]	2.11~2.17 and 2.4~2.5	9×20.5 (0.63λ×1.4λ@2.11 GHz)	25 and 20 @-20	-20/3700
[11]	5.1~5.8	10×16 (1.7λ×2.72λ@5.1 GHz)	56.1@16.5	16.5/100
[12]	2-18	18.5×18 (0.12λ×0.12λ@ 2GHz)	20@0.1m W/cm^2	0.1mW/cm^2 /100
[13]	0.9~1.1 and 1.8~2.5	21.3×6.4 (0.64λ×0.19λ@ 0.9 GHz)	75@20	0~23 /200~2000
This work	0.9~3	20×6 (0.6λ×0.18λ@0.9 GHz))	73.4@3	0~6 /800~1500

The performance of the proposed rectenna is compared with some recently published broadband (multifrequency band) rectennas including rectifiers, as shown in Table II. Our design can achieve high conversion efficiency ($\eta_c > 50\%$) at the widest frequency range (FBW about 107.7% at input power of 3 dBm and 102.7% at doubled or halved input power of 3 dBm). Although the load/input power range for high conversion efficiency is not the widest, both the load and input power can be tuned to maintain high conversion efficiency. For UWB matching between the antenna and nonlinear rectifier, due to the frequency dependence of *LC* resonating tank structure, the traditional multibranch complex matching stubs can be effectively simplified to a single matching stub with a compact size. Besides, the lossy switch can be avoided,

and high efficiency can be achieved, which is comparable with other broadband rectennas and rectifiers at the same input power level. Evidently, the proposed rectenna is highly efficient, much simpler, and relatively compact. To expand this design to lower power levels (for ambient RF energy harvesting at weak signal levels), zero-biased low-power high-frequency diodes (e.g., SMS7630, spin-diodes) could be used to substitute the selected diodes HSMS285X. In this case, the matching circuit including the frequency-dependent matching stub with *LC* tank will need to be further modified to accommodate the impedance variations of different nonlinear rectifier diodes for impedance complementary. Although the maximum conversion efficiency of this design may decrease to lower than 50% at low input powers, the conversion efficiency would maintain stable within the broadband frequency band, compared with the state-of-the-art broadband rectennas at low input power [10], [12]. Besides, it is already known that most diodes are generally of capacitive impedance, which has a similar trend (but different value ranges) for impedance versus frequency. Therefore, the proposed method could be universal for covering various UWB rectenna designs. The complex design for the receiving antenna and rectifying circuit is not required, and it can be used for general broadband antenna and rectifying circuit with typical structures. Hopefully, more UWB nonlinear co-design examples will be emerged by using the presented design method.

IV. Conclusion

A UWB rectenna has been proposed for MPT and energy harvesting. Due to the frequency dependence of the proposed *LC* resonant structure, the matching stub becomes a frequency-adjustable stub to achieve the impedance complementary between the antenna and the rectifying circuit. The demand for extra switching diodes and multiple matching branches has been eliminated, thereby improving the simplicity and miniaturization of such UWB rectennas and circuitry size significantly. The design method of this rectenna can be further developed to cover other broadband circuits and broadband nonlinear devices (e.g., power amplifiers). Also, the design method can be used to design the frequency reconfigurable structure for avoiding the switches, by replacing the active switches and varactors with the passive *LC* tanks.

References

[1] Z. Zhang, H. Pang, A. Georgiadis, and C. Cecati, "Wireless power transfer-an overview," *IEEE Trans. Ind. Electron.*, vol. 66, no. 2, pp. 1044–1058, Feb. 2019.

[2] T. Ngo, A.-D. Huang, and Y.-X. Guo, "Analysis and design of a reconfigurable rectifier circuit for wireless power transfer," *IEEE Trans. Ind. Electron.*, vol. 66, no. 9, pp. 7089–7098, Sep. 2019.

[3] F.-J. Huang, C.-M. Lee, C.-L. Chang, L.-K. Chen, T.-C. Yo, and C.-H. Luo, "Rectenna application of miniaturized implantable antenna design for triple-band biotelemetry communication," *IEEE Trans. Antennas Propag.*, vol. 59, no. 7, pp. 2646–2653, Jul. 2011.

[4] S. Shen, C.-Y. Chiu, and R. D. Murch, "Multiport pixel rectenna for ambient RF energy harvesting," *IEEE Trans. Antennas Propag.*, vol. 66, no. 2, pp. 644–656, Feb. 2018.

[5] H. Ye and Q.-X. Chu, "A broadband rectenna for harvesting low-power RF energy," in *Proc. ISAP*, Okinawa, Japan, 2016, pp. 46–47.

[6] H. S. Park and S. K. Hong, "Broadband RF-to-DC rectifier with uncomplicated matching network," *IEEE Microw. Wireless Compon. Lett.*, vol. 30, no. 1, pp. 43–46, Jan. 2020.

[7] M. M. Mansour and H. Kanaya, "High-efficient broadband CPW RF rectifier for wireless energy harvesting," *IEEE Microw. Wireless Compon. Lett.*, vol. 29, no. 4, pp. 288–290, Apr. 2019.

[8] C. Song, Y. Huang, J. Zhou, J. Zhang, S. Yuan, and P. Carter, "A high efficiency broadband rectenna for ambient wireless energy harvesting," *IEEE Trans. Antennas Propag.*, vol. 63, no. 8, pp. 3486–3495, May 2015.

[9] H. Sun, Y.-X. Guo, M. He, and Z. Zhong, "A dual-band rectenna using broadband Yagi antenna array for ambient RF power harvesting," *IEEE Antennas Wireless Propag. Lett.*, vol. 12, pp. 918–921, 2013.

[10] S. Shen, C.-Y. Chiu, and R. D. Murch, "A broadband L-probe microstrip patch rectenna for ambient RF energy harvesting," in *Proc. IEEE Int. Symp. Antennas Propag.*, Jul. 2017, pp. 2037–2038.

[11] P. Lu, X.-S. Yang, J.-L. Li, and B.-Z. Wang, "Polarization reconfigurable broadband rectenna with tunable matching network for microwave power transmission," *IEEE Trans. Antennas Propag.*, vol. 64, no. 3, pp. 1136–1141, Mar. 2016.

[12] J. A. Hagerty, F. B. Helmbrecht, W. H. McCalpin, R. Zane, and Z. B. Popovic, "Recycling ambient microwave energy with broad-band rectenna arrays," *IEEE Trans. Microw. Theory Techn.*, vol. 52, no. 3, pp. 1014–1024, Mar. 2004.

[13] C. Song *et al.*, "Matching network elimination in broadband rectennas for high-efficiency wireless power transfer and energy harvesting," *IEEE Trans. Ind. Electron.*, vol. 64, no. 5, pp. 3950–3961, May 2017.

[14] F. Jiang, C.-Y. Chiu, S. Shen, Q. S. Cheng, and R. Murch, "Pixel antenna optimization using N-port characteristic mode analysis," *IEEE Trans. Antennas Propag.*, vol. 68, no. 5, pp. 3336–3347, May 2020.

[15] P. Lu, X. S. Yang, J. L. Li, and B. Z. Wang, "A compact frequency reconfigurable rectenna for 5.2- and 5.8-GHz wireless power transmission," *IEEE Trans. Power Electron.*, vol. 30, no. 11, pp. 6006–6010, Nov. 2015.

[16] M. N. Srifi, S. K. Podilchak, M. Essaaidi, and Y. M. M. Antar, "Compact disc monopole antennas for current and future ultrawideband (UWB) applications," *IEEE Trans. Antennas Propag.*, vol. 59, no. 12, pp. 4470–4480, Dec. 2011.

[17] M. John and M. J. Ammann, "Optimization of impedance bandwidth for the printed rectangular monopole antenna," *Microw. Opt. Technol. Lett.*, vol. 47, no. 2, pp. 153–154, Oct. 2005.

[18] X. L. Bao and M. J. Ammann, "Investigation on UWB printed monopole antenna with rectangular slitted groundplane," *Microw. Opt. Technol. Lett.*, vol. 49, no. 7, pp. 1585–1587, Jul. 2007.

[19] S. Kumar and M. Kumar, "RF power divider for CDMA, Bluetooth & 3G application using stepped-impedance technology," in *Proc. Int. Conf. Adv. Eng. Technol. Res.*, Unnao, India, Aug. 2014, pp. 1–5.

[20] J. Liang, C. C. Chiau, X. Chen, and C. G. Parini, "Study of a printed circular disc monopole antenna for UWB systems," *IEEE Trans. Antennas Propag.*, vol. 53, no. 11, pp. 3500–3504, Nov. 2005.

[21] B. Allen, M. Dohler, E. Okon, W. Malik, A. Brown, and D. Edwards, *Ultra Wideband Antennas and Propagation for Communications, Radar and Imaging*. Hoboken, NJ, USA: Wiley, 2007.

[22] R. Garg, P. Bhartia, I. Bahl, and A. Ittipiboon, *Microstrip Antenna Design Handbook*. Norwood, MA, USA: Artech House, 2001.

[23] T. Peter, S. W. Cheung, S. K. A. Rahim, and A. R. Tharek, "A grounded CPW transparent UWB antenna for UHF and microwave frequency application," in *Proc. Prog. Electromagn. Res. Symp. Process.*, Taipei, Taiwan, 2013, pp. 479–481.

[24] Q. Xu, Y. Huang, X. Zhu, L. Xing, Z. Tian, and C. Song, "A modified two-antenna method to measure the radiation efficiency of antennas in a reverberation chamber," *IEEE Antennas Wireless Propag. Lett.*, vol. 15, pp. 336–339, 2016.

[25] Hewlett Packard Technologies. (1998). *HSMS 2850, Surface Mount RF Schottky Barried Diodes*. [Online]. Available: http://www.hp.Woodshot.com/hprfhelp/4_downld/products/diodes/hsms2850

[26] R. M. Fano, "Theoretical limitations on the broadband matching of arbitrary impedances," *J. Franklin Inst.*, vol. 249, no. 2, pp. 139–154, Feb. 1950.

[27] E. Schwartz, "Broadband matching of resonant circuits and circulators," *IEEE Trans. Microw. Theory Techn.*, vol. 16, no. 3, pp. 158–165, Mar. 1968.

[28] R. Grossbach, "Design considerations for thick-film high power chip terminations," *Microw. J. Euroglobal Ed.*, vol. 43, no. 11, pp. 86–104, 2000.

[29] T.-W. Yoo and K. Chang, "Theoretical and experimental development of 10 and 35 GHz rectennas," *IEEE Trans. Microw. Theory Techn.*, vol. 40, no. 6, pp. 1259–1266, Jun. 1992.
[30] B. R. Alam, "Broadband performance of multi-section step-line impedance matching of LD-MOSFET RF amplifier at 900 MHz LTE band," in *Proc. Int. Conf. Electr. Eng. Informat. (ICEEI)*, Bali, IN, USA, Aug. 2015, pp. 336–340.
[31] M. David Pozar, *Microwave Engineering*. New York, NY, USA: Wiley, 2011.
[32] P. Lu, C. Song, and K. M. Huang, "A two-port multipolarization rectenna with orthogonal hybrid coupler for simultaneous wireless information and power transfer (SWIPT)," *IEEE Trans. Antennas Propag.*, vol. 68, no. 10, pp. 6893–6905, Oct. 2020.

Ping Lu (Member, IEEE) received the B.S. degree in electrical engineering and automation from Southwest Jiaotong University, Chengdu, China, in 2012, and the Ph.D. degree in radio physics from the University of Electronic Science and Technology, Chengdu, in 2018.

From 2015 to 2017, she was a Joint Ph.D. Student Scholar at the Laboratoire Ampére, École Centrale de Lyon, INSA de Lyon, Université Claude Bernard de Lyon, Villeurbanne, France. She is currently an Assistant Professor with the School of Electronics and Information Engineering, Sichuan University, Chengdu. Her current research interests include rectenna, nondiffraction beams, and wireless power transmission.

Chaoyun Song (Member, IEEE) received the B.Eng., M.Sc. (with distinction), and Ph.D. degrees in electrical engineering and electronics from The University of Liverpool (UoL), Liverpool, U.K., in 2012, 2013, and 2017, respectively.

He was a Post-Doctoral Research Associate with UoL, from 2017 to 2020. He is currently an Assistant Professor with the School of Engineering and Physical Sciences (EPS), Heriot-Watt University, Edinburgh, U.K. He has authored more than 70 articles (including 30 IEEE Transactions) in peer-reviewed journals and conference proceedings. He holds five U.S., European, and U.K. patents. His current research interests include liquid antennas, material science, wireless energy harvesting, rectifying antennas (rectennas), wireless power transfer, metamaterials and metasurface, and smart sensors for the internet of things.

Dr. Song was a recipient of many international awards such as the winner of the IET Present Around the World Competition in 2016, the EW Bright-Sparks Award for Top 30 U.K. electronic engineers under age 30 in 2018, and the BAE Systems Chairman's Award in 2017 for the innovation of the next-generation global navigation satellite system antennas. He received the Highly Commended Award from the prestigious IET innovation awards over three categories—"Energy and Power," "Emerging Technologies," and "Young Innovators" in 2018. He is a regular reviewer for more than 20 international journals including *Nature Communications* and seven IEEE Transactions and a Guest Editor of the *Wireless Communications and Mobile Computing*.

Ka Ma Huang (Senior Member, IEEE) was born in Chongqing, China, in 1964. He received the M.S. and Ph.D. degrees in microwave theory and technology from the University of Electronic Science and Technology, Chengdu, China, in 1988 and 1991, respectively.

In 1996, 1997, 1999, and 2001, he was a Visiting Scientist with the Scientific Research Center Vidhuk, Kyiv, Ukraine, the Institute of Biophysics CNR, Genoa, Italy, Technical University Vienna, Vienna, Austria, and Clemson University, Clemson, SC, USA, where he cooperated with the scientists to study the interaction between electromagnetic fields and complex media in biological structure and reaction systems. Since 1994, he has been a Professor with the Department of Radio and Electronics, Sichuan University, Chengdu, where he has been the Director of the department since 1997. He has authored or coauthored more than 100 articles. His current research interests include microwave chemistry and electromagnetic theory.

Dr. Huang was a recipient of several research awards from the Chinese Government.